ACS OMEGA

Article

Cite This: ACS Omega 2018, 3, 1939−1945

Dye-Assisted Transformation of Cu_2O Nanocrystals to Amorphous Cu_xO Nanoflakes for Enhanced Photocatalytic Performance

Yang Su,[†] Hongfei Li,[†] Hanbin Ma,[†] Hua Wang,[‡] John Robertson,[†] and Arokia Nathan*[,†]

[†]Department of Engineering, University of Cambridge, Cambridge CB3 0FA, U.K.

[‡]Jiangsu Province Environment Monitoring Centre, Nanjing 210036, China

Supporting Information

ABSTRACT: Amorphous Cu_xO nanoflakes with a thickness of 10−50 nm were synthesized through dye-assisted transformation of rhombic dodecahedral Cu_2O nanocrystals using a facile solution process. The morphology evolution observed by electron microscopy is highly dependent on the reaction between the surface and the dye. The crystal grain shrinks during the process until the formation of a purely amorphous nanoflake. The amorphous Cu_xO nanoflake consists of a combination of Cu(I) and Cu(II) with a ratio close to 1:1. It shows enhanced photocatalytic reactivity toward the degradation of methyl orange compared to that of rhombic dodecahedral Cu_2O nanocrystals with all active (110):Cu facets. The chemical composition and architecture remain the same after repeating degradation tests. The high surface-to-volume ratio contributes to its superior photocatalytic performance, whereas its low surface energy, confirmed by density functional theory simulations, explains its improved stability. The nanoflakes also show the ability of degrading nitrobenzene effectively, thus demonstrating great promise as a highly stable and active photocatalyst for environmental applications.

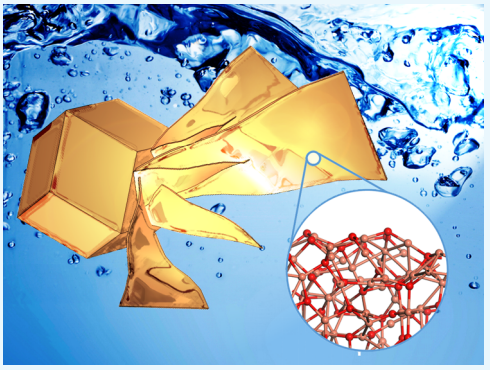

INTRODUCTION

Cupric oxide (CuO) and cuprous oxide (Cu_2O) have raised significant research interests recently because of their promising applications in hydrogen production,[1,2] carbon dioxide reduction,[3] solar energy conversion,[4] water purification,[5] and other photocatalytic applications.[6−11] Indeed, Cu_2O photocatalysts for wastewater purification have demonstrated high efficiency, low toxicity, and environmental acceptability.[12] They are typically p-type semiconductors with a narrow band gap, and their structure- and facet-dependent properties have been studied in detail.[13] The major drawback of Cu_2O photocatalysts lies in the poor stability under irradiation,[14] limiting their long-term photocatalytic applications. Many studies have been carried out to improve the photocatalytic activity and stability of Cu_2O photocatalysts by introducing a cocatalyst to form a composite photocatalyst.[5,10,15−18] Apart from photocorrosion, Cu_2O photocatalysts are also reported to suffer from reconstruction during the photocatalytic reaction.[12,19] Compared with Cu_2O photocatalysts, CuO shows good stability but much lower photocatalytic reactivity. This is due to its small band gap and the easy recombination of electron−hole pairs, thus limiting its ability of initiating photocatalytic reactions. The preparation of copper oxide-based photocatalysts with high reactivity and stability remains challenging. To achieve better photocatalytic performance, nanostructures with high surface-to-volume ratios are highly desired. Numerous works on copper oxide nano- or microparticles of various structural topologies have been reported.[20−24] Hollow cages and other topologies with a larger specific surface area have also been synthesized.[25−27] The synthesis of one-dimensional (e.g., nanowire) or two-dimensional (e.g., nanoflake) architectures with even higher surface-to-volume ratios has hitherto remained a challenge. Cu_xO or CuO_x is a hybrid of Cu(I) and Cu(II). Indeed, Cu_4O_3 (paramelaconite) is the most typical Cu_xO material with 50% Cu(I) and 50% Cu(II).[28] Cu_xO is difficult to synthesize from the standpoint of stabilizing both Cu(I) and Cu(II) at the same time.[29]

In this work, we take advantage of dye-assisted transformation of Cu_2O nanocrystals to form amorphous Cu_xO nanoflakes for the first time. The preparation was carried out using a facile solution process. We study in detail the evolution process and the underlying mechanism along with an analysis of the atomic structure and surface energy using density functional theory (DFT) simulations. The as-obtained amorphous Cu_xO nanoflakes show enhanced photocatalytic reactivity toward the degradation of methyl orange under irradiation by visible-light light-emitting diodes (LEDs). The amorphous Cu_xO nanoflakes demonstrate good stability after numerous degradation test cycles without much change in either morphology or chemical composition and even seem to very effectively degrade nitrobenzene. The results suggest that

Received: October 21, 2017
Accepted: November 29, 2017
Published: February 14, 2018

DOI: 10.1021/acsomega.7b01612
ACS Omega 2018, 3, 1939−1945

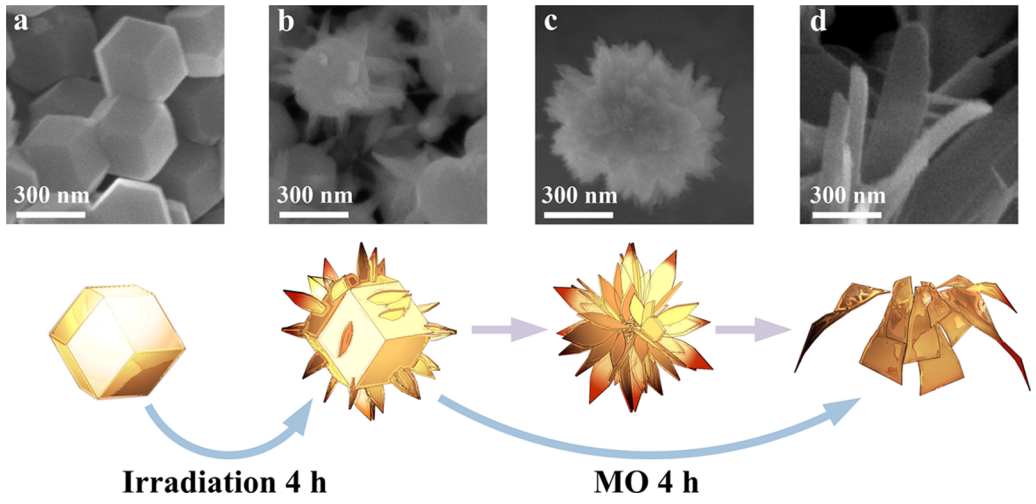

Figure 1. Morphology evolution from a rhombic dodecahedral nanostructure to a nanoflake. SEM images of the (a) original Cu_2O rhombic dodecahedral nanocrystal, (b) rhombic dodecahedral structure with nanosheets on the surface after 4 h of irradiation in deionized water, (c) flowerlike intermediate structure, and (d) nanoflake structure after 4 h of immersion in methyl orange solution under irradiation.

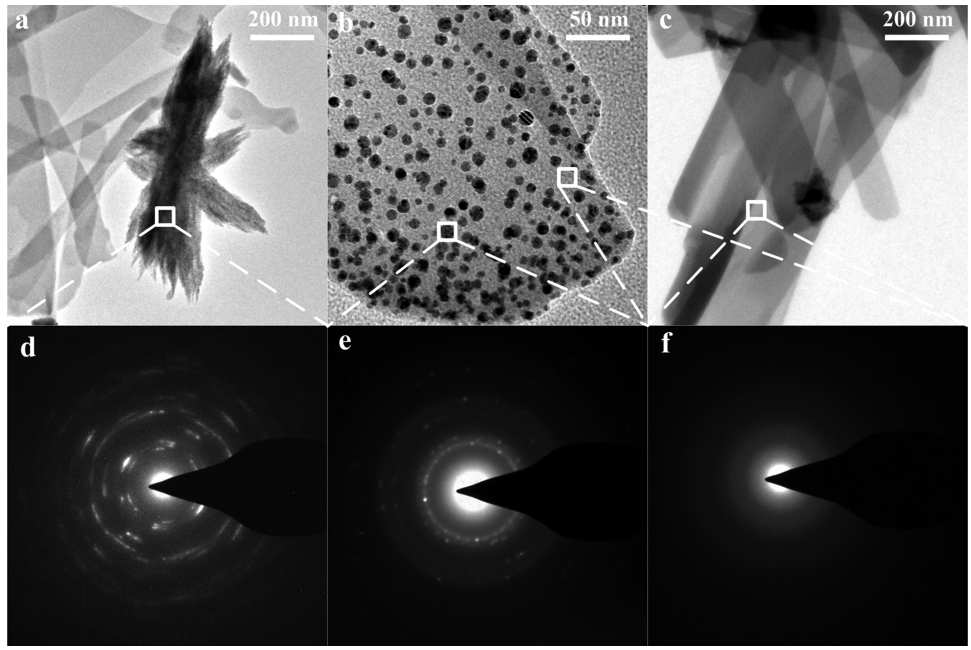

Figure 2. TEM images of the (a) flowerlike structure, (b) amorphous nanoflake with dispersed crystal grains, and (c) amorphous nanoflake. SAED patterns of the (d) flowerlike structure, (e) crystal grain, and (f) amorphous nanoflake.

Cu_xO with amorphous nanoflake topology is very promising as a high-efficiency and stable photocatalyst for wastewater purification.

RESULTS AND DISCUSSION

Evolution of Morphology and Crystallization. The evolution of morphology was observed using scanning electron microscopy (SEM), as shown in Figure 1. Cu_2O nanocrystals with a rhombic dodecahedral nanostructure (Figure 1a) were dispersed in deionized water and stirred constantly under irradiation with LED as a light source for 4 h. The spectra of the LED light source are shown in Figure S1, and its electrical power is measured to be 8.880 W. No UV component (wavelength < 400 nm) is detected, and the peak is located at 455 nm. After 4 h of irradiation, some nanosheets grew on the surface, as presented in Figure 1b. A flowerlike intermediate structure, as shown in Figure 1c, could be observed after methyl orange was introduced to the solution. The morphology finally transformed to nanoflake (Figure 1d) after 4 h of irradiation in methyl orange solution. The length of nanoflakes ranged from 100 nm to a few micrometers with thickness between 10 and 50 nm, as measured with SEM. The irradiation by the LED light source is critical for this evolution. Quite a few nanoflakes were formed without 4 h of irradiation in deionized water, as shown in Figure S2a. The yield of nanoflakes is comparably low without 4 h of irradiation in methyl orange solution, as presented in Figure S2b, indicating that irradiation at this stage accelerates the evolution process. Cubic and octahedral Cu_2O nanocrystals were tested under the same conditions, and the flake yield followed the sequence of cube < octahedron < rhombic dodecahedron, as demonstrated in Figure S3. This is consistent with the associated photo-

DOI: 10.1021/acsomega.7b01612
ACS Omega 2018, 3, 1939−1945

catalytic reactivity reported in our previous work.[31] Congo red, methylene blue, and rhodamine B were used as a replacement of methyl orange, and the flake yield observed by SEM is presented in Figure S4. Quite a few nanoflakes were formed using methylene blue and rhodamine B. Although flakes were observed with Congo red, the yield is much lower compared to that using methyl orange. These observations show that the photocatalytic interaction between the dye and the Cu_2O photocatalyst is critical for the formation of nanoflakes. Rhombic dodecahedron Cu_2O nanocrystals, which show the highest photocatalytic activity toward the degradation of methyl orange, generate the most nanoflakes, whereas cubic Cu_2O nanocrystals generate the least. The high density of terminal copper atoms makes the $Cu_2O(110)$ facet positively charged, as demonstrated in Figure S5. The $Cu_2O(110)$ facet electrostatically repels the positively charged methylene blue and rhodamine B molecules, whereas the negatively charged methyl orange and Congo red molecules are adsorbed to the surface easily.

The evolution of crystallization was studied using transmission electron microscopy (TEM), as presented in Figure 2. The flowerlike intermediate structure in Figure 2a and its corresponding selective area electron diffraction (SAED) pattern in Figure 2d indicate that it remains crystalline in structure. The magnified TEM image of the tip of the flowerlike structure is demonstrated in Figure 2b. The tip consists of two components, including small grains in dark gray and flat areas in light gray. The magnified TEM image of the flowerlike structure and its energy-dispersive X-ray spectroscopy are shown in Figure S6. The flowerlike structure contains 64.27% Cu and 35.73% O. The SAED pattern of grains, as shown in Figure 2e, denotes their crystal structure, whereas the SAED pattern of the flat area in Figure 2f shows an amorphous phase. The uniform nanoflake in Figure 2c has the same SAED pattern (Figure 2f) as that of the flat area in Figure 2b, confirming that it is completely amorphous. It can be concluded that the transformation from crystal to amorphous begins from the tips and the size of the crystal grains reduces continuously until the entire structure becomes an amorphous nanoflake.

Characterization of Nanomaterials. The phase of products was determined by X-ray diffraction (XRD) measurements, as shown in Figure 3a. The same amount of products was used. Rhombic dodecahedral Cu_2O nanocrystals show a typical Cu_2O pattern, whereas the peaks decline dramatically as the transformation process continues, indicating a weaker crystallization phase and the formation of the amorphous structure. The XRD pattern of the nanoflakes is almost a flat line, although the presence of weak peaks shows a small fraction of untransformed nanocrystals. The UV−vis absorption spectra of the rhombic dodecahedral Cu_2O nanocrystal and amorphous nanoflake are presented in Figure 3b. The rhombic dodecahedral Cu_2O nanocrystal has an absorption peak at 455 nm, and the characteristic light-scattering feature from 500 to 1100 nm is due to the large particle size. Nanoflakes show strong absorption from 380 to 500 nm, and no light scattering is observed. The chemical composition was studied using X-ray photoelectron spectroscopy (XPS) measurements. The XPS patterns of various products are shown in Figure 3c, and the baseline has been subtracted. The XPS pattern of the rhombic dodecahedral Cu_2O nanocrystal shows peaks of only Cu $2p_{1/2}$ (952.28 eV) and Cu $2p_{3/2}$ (932.38 eV), implying a +1 chemical valence of Cu in the product. After 4 h of irradiation in deionized water, the main peak becomes wider and the shakeup peak appears, indicating

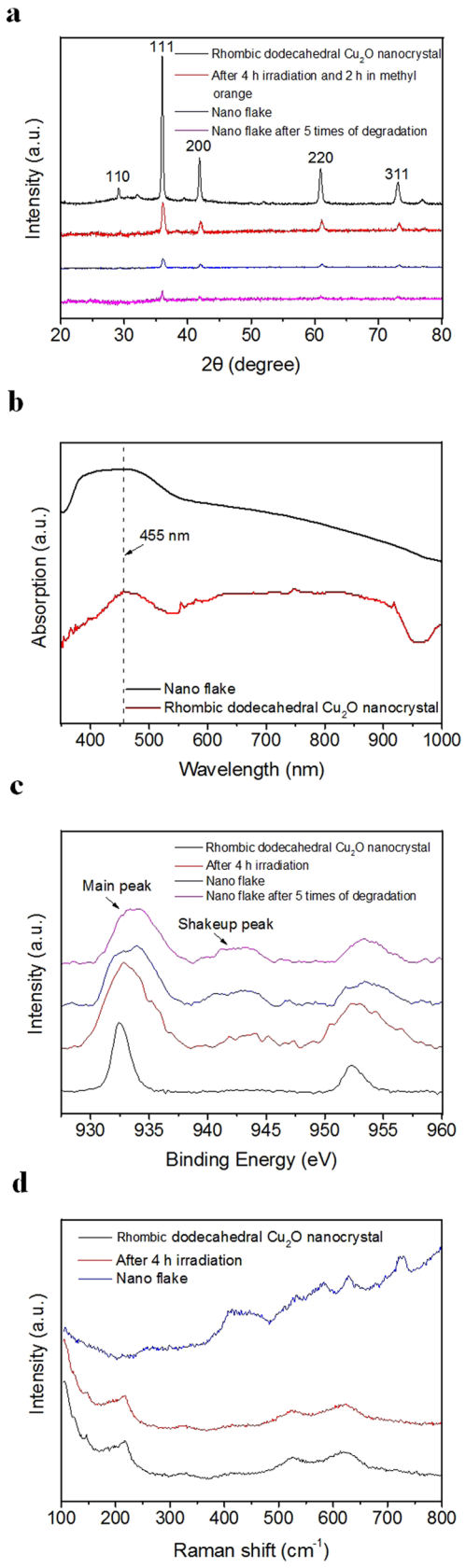

Figure 3. (a) XRD patterns, (b) UV−vis absorption spectra, (c) XPS patterns, and (d) Raman spectra of the as-obtained samples.

DOI: 10.1021/acsomega.7b01612
ACS Omega 2018, 3, 1939−1945

the existence of +2 chemical valence of Cu. The main peak contains contributions from both Cu(I) and Cu(II), whereas the shakeup peak entirely comes from Cu(II). The Cu(I) and Cu(II) ratios can be calculated according to the following equations[32]

$$\%\ \mathrm{Cu(I)} = (A - (A_1/B)B)/(A + B) \times 100 \quad (1)$$

$$\%\ \mathrm{Cu(II)} = B(1 + (A_1/B))/(A + B) \times 100 \quad (2)$$

where A is the total area of the main peak and B is the area of the shakeup peak. A_1/B is the ratio of the direct photoemission (A_1) and the shakeup photoemission (B) of Cu(II). It was found to be 1.59 ± 0.1 in this work. After 4 h of irradiation in deionized water, the Cu(I) and Cu(II) ratios reach 61.4 and 38.6%, respectively. The Cu(II) ratio of the nanoflake increases to 52.4%, indicating that both Cu(I) and Cu(II) exist in the products. The increase of the Cu(II) ratio implies that some Cu(I) atoms are oxidized to Cu(II) during the photocatalytic reaction between methyl orange and the postirradiation rhombic dodecahedral Cu_2O nanocrystal. The Raman spectra are demonstrated in Figure 3d. The spectra of rhombic dodecahedral Cu_2O nanocrystals agree well with those in the literature.[33,34] After 4 h of irradiation, the Raman spectra do not change significantly, indicating that the majority composition is still Cu_2O. The Raman spectra of Cu_xO nanoflakes formed after 4 h of irradiation in methyl orange solution are completely different from those of Cu_2O, CuO, or Cu_4O_3,[35] confirming the complete transformation of rhombic dodecahedral Cu_2O nanocrystals and the new phase of amorphous Cu_xO nanoflakes.

Photocatalysis Performance. Figure 4a compares the degradation of methyl orange using the rhombic dodecahedral Cu_2O nanocrystal and amorphous Cu_xO nanoflake photocatalysts. The degradation reaches 74.1% after 30 min of constant stirring without irradiation using the amorphous Cu_xO nanoflake. This is due to the strong chemical adsorption between the surface and the sulfonate group (SO_3^-) of methyl orange.[19] The removal of methyl orange reaches 93.2% after 30 min of photocatalytic reaction, and no methyl orange is detected after 2 h of photocatalytic degradation. The photocatalytic reaction obeys pseudo-first-order kinetics, and the first-order rate constant, K_{app}, can be calculated using the following equation

$$\ln(C/C_0) = -K_{app}t \quad (3)$$

where C/C_0 is the degradation of methyl orange and t is the degradation time. Thus, K_{app} values for amorphous Cu_xO nanoflakes and rhombic dodecahedral Cu_2O nanocrystals are calculated to be 2.72 and 1.67 h^{-1}, respectively. The surface area is studied on the basis of Brunauer–Emmett–Teller (BET) theory, and respective plots are depicted in Figure S7. The BET surface area of the amorphous Cu_xO nanoflake is measured to be 36.3987 m^2/g, whereas that of the rhombic dodecahedral Cu_2O nanocrystal is only 4.7804 m^2/g. The high surface-to-volume ratio of amorphous Cu_xO nanoflakes also contributes to its high photocatalytic activity. The photocatalytic performance of amorphous Cu_xO nanoflakes is compared to that reported in other studies, as listed in Table S1. The photocatalytic stability is tested by cycling degradation of methyl orange, as demonstrated in Figure 4b. The degradation rate remains almost the same after five repeated degradation cycles, indicating good stability of the amorphous Cu_xO nanoflake. Cu_2O photocatalysts are known to suffer from photocorrosion.[36] Cu(I) is oxidized to Cu(II) during photocatalysis, and the photocatalytic activity declines, thus limiting the lifetime of the Cu_2O photocatalyst. The SEM image of the amorphous Cu_xO nanoflake after repeating tests is presented in Figure S8. The nanoflake keeps its original structure after cycling degradation tests. The XRD and XPS patterns of amorphous Cu_xO nanoflakes are shown in Figure 3a,c. The XRD pattern remains unchanged, whereas the Cu(II) ratio increases only slightly to 54.4%, confirming the high stability of the amorphous Cu_xO nanoflake. Nitrobenzene, which is a stable and toxic organic compound in industrial wastewater, is also used to test the photocatalytic reactivity of the amorphous

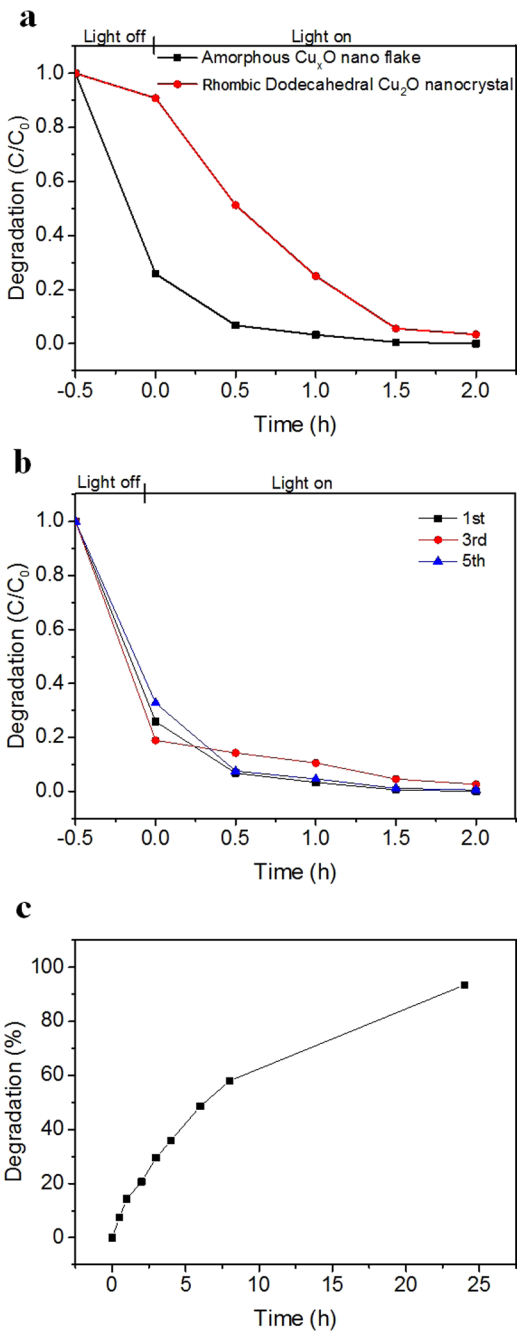

Figure 4. (a) Methyl orange degradation with amorphous Cu_xO nanoflakes and rhombic dodecahedral Cu_2O nanocrystals. (b) Repeated methyl orange degradation tests. (c) Nitrobenzene degradation test.

DOI: 10.1021/acsomega.7b01612
ACS Omega 2018, 3, 1939−1945

Cu_xO nanoflake. After 24 h of continuous photocatalytic reaction, 93.5% of the nitrobenzene is degraded, as shown in Figure 4c. No organics are detected in the end, as confirmed by the total ion chromatogram plots and mass spectrum, as shown in Figure S9, indicating that the final products are carbon dioxide and water.

Atomic Structure and Surface Energy. The atomic structure and surface of amorphous Cu_xO are shown in Figure 5. Different from the structure of crystal CuO or Cu_2O, most

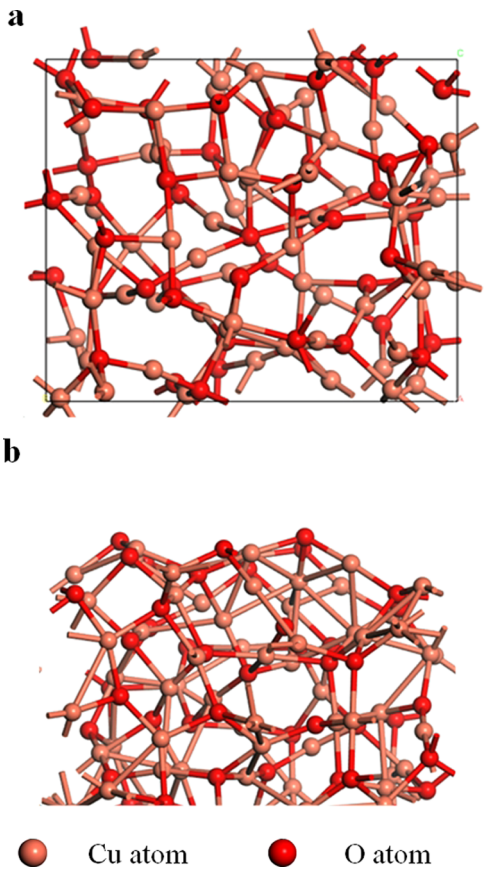

Figure 5. (a) Atomic structure and (b) surface of amorphous Cu_xO.

of the Cu atoms of amorphous Cu_xO are 3-fold, whereas a small portion is 2- or 4-fold. On the other hand, most O atoms are 4-fold. The amorphous Cu_xO surface structure is cleaved from the amorphous Cu_xO structure and then fully relaxed. The surface contains Cu and O atoms; thus, both O and Cu dangling bonds appear on this surface. Our previous paper[31] showed that O-terminated surfaces tend to be energetically stable, whereas the Cu-terminated surfaces tend to be more photocatalytically active. The amorphous Cu_xO nanoflake, transformed from the rhombic dodecahedral Cu_2O nanocrystal with all (110):Cu facets, is known to be highly photocatalytically active. The surface energy of the amorphous Cu_xO surface is calculated and compared to that of the $Cu_2O(110)$ surfaces, as shown in Table 1. The amorphous Cu_xO surface has a much smaller surface energy than that of the $Cu_2O(110)$ stoichiometric and Cu-terminated surfaces and hence has much better stability. In addition, the exposed Cu atoms with dangling bonds on the amorphous Cu_xO surface play an important role in photocatalytic reactions, leading to high reactivity. As a result, the amorphous Cu_xO nanoflake shows

Table 1. Surface Free Energy of Amorphous Cu_xO and $Cu_2O(110)$ Surfaces

surface model	amorphous Cu_xO	$Cu_2O(110)$ stoichiometric	$Cu_2O(110)$:Cu
surface energy ($eV/Å^2$)	0.022	0.058	0.115–0.118

good stability and high photocatalytic reactivity at the same time.

CONCLUSIONS

Amorphous Cu_xO nanoflakes have been synthesized by transforming rhombic dodecahedral Cu_2O nanocrystals, taking advantage of dye-assisted transformation. The morphology evolution has several stages, including the original rhombic dodecahedral nanocrystal, rhombic dodecahedral structure with nanosheets on the surface, flowerlike intermediate structure, and finally nanoflakes. The size of the crystal grains reduces gradually during the transformation until the formation of the purely amorphous nanoflakes. The categories of dyes and the photocatalytic activity of the original nanocrystals have a great effect on the evolution process. Rhombic dodecahedral Cu_2O nanocrystals generate the most Cu_xO nanoflakes compared with other morphologies. The amorphous Cu_xO shows an absorption peak at around 455 nm, and the XRD measurements confirm the nature of the amorphous structure. The ratio of Cu(I) and Cu(II) calculated by XPS measurements is close to 1:1. The as-obtained amorphous Cu_xO nanoflakes show higher photocatalytic reactivity toward the degradation of methyl orange compared to that of rhombic dodecahedral Cu_2O nanocrystals with all active (110):Cu facets. The nanoflakes having a much lower surface energy demonstrate good structural stability and chemical composition with the exposed Cu atoms with dangling bonds despite repeated degradation tests. They are also effective in degrading nitrobenzene. The results presented here demonstrate a new copper oxide nanomaterial structure and a new facile way of preparing a highly active and stable photocatalyst for environmental applications.

EXPERIMENTAL SECTION

Chemicals. The chemicals used, that is, copper(II) chloride (97%), hydroxylamine hydrochloride (99%), sodium dodecyl sulfate (SDS) (98.5%), methyl orange (100%), methylene blue (82%), Congo red (85%), and rhodamine B (95%), were purchased from Sigma-Aldrich. Sodium hydroxide (98%) was purchased from Fisher brand. All chemicals were used as received without further purification.

Synthesis of Cu_2O Nanocrystals. Cu_2O nanocrystals were synthesized using a simple solution process as reported in our previous work.[30] Sixty-seven milligrams of $CuCl_2$ and 1 g of SDS were dispersed in 65 mL of deionized water. The solution was placed in a water bath at 35 °C with vigorous stirring for 10 min. Ten milliliters of 0.2 M NaOH was introduced. Cubic, octahedral, and rhombic dodecahedral nanostructures were obtained by introducing 25 mL of 0.17, 0.4, and 1.0 M $NH_2OH{\cdot}HCl$, respectively. The solution was stirred for 30 s and kept in the water bath for 1 h. The products were centrifuged at 5000 rpm for 4 min, and the precipitate was washed and centrifuged twice using 50 mL of water and ethanol. The obtained products were dried in an oven at 60 °C for 12 h.

DOI: 10.1021/acsomega.7b01612
ACS Omega 2018, 3, 1939−1945

Synthesis of Amorphous Cu_xO Nanoflakes. One portion of the as-prepared Cu_2O nanocrystal was dispersed in 250 mL of deionized water. The solution was constantly stirred under irradiation with a visible LED light source for 4 h. Ten milligrams of methyl orange was then introduced, and the solution was stirred for another 4 h under irradiation. The products were centrifuged at 5000 rpm for 4 min, and the precipitate was washed and centrifuged twice using 50 mL of water and ethanol. The resulting products were dried in an oven at 60 °C for 12 h.

Nanomaterial Characterization. The morphologies of the synthesized nanomaterial were studied using LEO Gemini 1530VP scanning electron microscopy (SEM) at 8 kV and FEI Tecnai G2 20 transmission electron microscopy (TEM) at 200 kV. Ultraviolet−visible (UV−vis) absorption spectra were recorded using a UniCam UV−vis spectrometer v.2. X-ray diffraction (XRD) patterns were obtained using a Bruker D8 Advance diffractometer with Cu Kα radiation. X-ray photoelectron spectroscopy (XPS) measurements were performed using a PHI5000VersaProbe II scanning XPS microscope. Raman spectra were obtained using a Renishaw inVia Raman microscope with the range from 100 to 800 cm^{-1}. The Brunauer−Emmett−Teller (BET) surface area was measured by Micromeritics Gemini VII.

Photocatalysis Experiments. White-light LEDs were used as the light source. The spectra of the light source were recorded using a Labsphere CDS-600 spectrometer. The photocatalysis experiment on the degradation of methyl orange was carried out in a homemade quartz immersion reactor with a volume of 300 mL at room temperature. Thirty milligrams of pristine Cu_2O nanocrystals or amorphous Cu_xO nanoflakes were dispersed in 250 mL of the 20 mg/L methyl orange solution. The solution was constantly stirred in the dark for 15 min to reach an adsorption−desorption equilibrium. Every 30 min, 1.5 mL of the solution was sampled and centrifuged at 5000 rpm for 4 min to separate the photocatalysts from the solution. The UV−vis absorption spectra of the samples were recorded, and the concentration of methyl orange was determined by the absorption at 464 nm using UniCam UV−vis spectrometer v.2. For the degradation of nitrobenzene solution, one portion of amorphous Cu_xO nanoflake photocatalysts (30 mg) was dispersed in 250 mL of the 30 mg/L nitrobenzene solution. The photocatalytic reaction was carried out in a 300 mL reactor under LED illumination and with vigorous magnetic stirring. The categories and concentrations of the organic compounds were studied using a Thermo Scientific DSQ II GC/MS system.

DFT Calculation. The calculations were carried out with plane-wave DFT code CASTEP using ultrasoft pseudopotentials and a plane-wave cutoff of 400 eV. This converged the energies to under 0.01 eV per atom. We generated a 112-atom (64 Cu and 48 O) random network supercell of Cu_xO by DFT molecular dynamics (MD). A heating MD process at 3000 K was applied first for 10 ps. Then, the network was slowly cooled down to 300 K at a quenching rate of 1 ps/100 K. Finally, geometry relaxation, including lattice parameter relaxation, was applied to the amorphous network to obtain the atomic structure. Our amorphous model gave a density of 5.61 g/cm^3.

■ ASSOCIATED CONTENT

Supporting Information

The Supporting Information is available free of charge on the ACS Publications website at DOI: 10.1021/acsomega.7b01612.

Spectra of LED light source, SEM images of nanocrystals under various conditions, illustration of interaction between the $Cu_2O(110)$ surface and dyes, BET plots, and SEM image of amorphous Cu_xO nanoflakes after repeated degradation tests (PDF)

■ AUTHOR INFORMATION

Corresponding Author

*E-mail: an299@cam.ac.uk.

ORCID

Yang Su: 0000-0001-5425-5920

Notes

The authors declare no competing financial interest.

■ ACKNOWLEDGMENTS

This work was funded by the Engineering and Physical Sciences Research Council under Project EP/M013650/1.

■ REFERENCES

(1) Yin, W.; Bai, L.; Zhu, Y.; Zhong, S.; Zhao, L.; Li, Z.; Bai, S. Embedding Metal in the Interface of a P-N Heterojunction with a Stack Design for Superior Z-Scheme Photocatalytic Hydrogen Evolution. *ACS Appl. Mater. Interfaces* **2016**, *8*, 23133−23142.

(2) Hong, J. W.; Wi, D. H.; Lee, S.-U.; Han, S. W. Metal-Semiconductor Heteronanocrystals with Desired Configurations for Plasmonic Photocatalysis. *J. Am. Chem. Soc.* **2016**, *138*, 15766−15773.

(3) Yu, L.; Li, G.; Zhang, X.; Ba, X.; Shi, G.; Li, Y.; Wong, P. K.; Yu, J. C.; Yu, Y. Enhanced Activity and Stability of Carbon-Decorated Cuprous Oxide Mesoporous Nanorods for CO2 Reduction in Artificial Photosynthesis. *ACS Catal.* **2016**, *6*, 6444−6454.

(4) Zuo, Z.; Ramírez, P. J.; Senanayake, S. D.; Liu, P.; Rodriguez, J. A. Low-Temperature Conversion of Methane to Methanol on CeOx/Cu2O Catalysts: Water Controlled Activation of the C-H Bond. *J. Am. Chem. Soc.* **2016**, *138*, 13810−13813.

(5) Xiong, J.; Li, Z.; Chen, J.; Zhang, S.; Wang, L.; Dou, S. Facile Synthesis of Highly Efficient One-Dimensional Plasmonic Photocatalysts through Ag@Cu2O Core-Shell Heteronanowires. *ACS Appl. Mater. Interfaces* **2014**, *6*, 15716−15725.

(6) Wang, B.; Durantini, J.; Nie, J.; Lanterna, A. E.; Scaiano, J. C. Heterogeneous Photocatalytic Click Chemistry. *J. Am. Chem. Soc.* **2016**, *138*, 13127−13130.

(7) Fishman, Z. S.; Rudshteyn, B.; He, Y.; Liu, B.; Chaudhuri, S.; Askerka, M.; Haller, G. L.; Batista, V. S.; Pfefferle, L. D. Fundamental Role of Oxygen Stoichiometry in Controlling the Band Gap and Reactivity of Cupric Oxide Nanosheets. *J. Am. Chem. Soc.* **2016**, *138*, 10978−10985.

(8) Hornés, A.; Hungría, A. B.; Bera, P.; López Cámara, A.; Fernández-García, M.; Martínez-Arias, A.; Barrio, L.; Estrella, M.; Zhou, G.; Fonseca, J. J.; Hanson, J. C.; Rodriguez, J. A. Inverse CeO2/CuO Catalyst as an Alternative to Classical Direct Configurations for Preferential Oxidation of CO in Hydrogen-Rich Stream. *J. Am. Chem. Soc.* **2010**, *132*, 34−35.

(9) Zahran, E. M.; Bedford, N. M.; Nguyen, M. A.; Chang, Y. J.; Guiton, B. S.; Naik, R. R.; Bachas, L. G.; Knecht, M. R. Light-Activated Tandem Catalysis Driven by Multicomponent Nanomaterials. *J. Am. Chem. Soc.* **2014**, *136*, 32−35.

(10) Li, J.; Cushing, S. K.; Bright, J.; Meng, F.; Senty, T. R.; Zheng, P.; Bristow, A. D.; Wu, N. Ag@Cu2O Core-Shell Nanoparticles as Visible-Light Plasmonic Photocatalysts. *ACS Catal.* **2013**, *3*, 47−51.

DOI: 10.1021/acsomega.7b01612
ACS Omega 2018, 3, 1939−1945

(11) Xu, H.; Feng, J.-X.; Tong, Y.-X.; Li, G.-R. Cu2O−Cu Hybrid Foams as High-Performance Electrocatalysts for Oxygen Evolution Reaction in Alkaline Media. *ACS Catal.* **2017**, *7*, 986−991.
(12) Zheng, Z.; Huang, B.; Wang, Z.; Guo, M.; Qin, X.; Zhang, X.; Wang, P.; Dai, Y. Crystal Faces of Cu2O and Their Stabilities in Photocatalytic Reactions. *J. Phys. Chem. C* **2009**, *113*, 14448−14453.
(13) Huang, W. C.; Lyu, L. M.; Yang, Y. C.; Huang, M. H. Synthesis of Cu2O Nanocrystals from Cubic to Rhombic Dodecahedral Structures and Their Comparative Photocatalytic Activity. *J. Am. Chem. Soc.* **2012**, *134*, 1261−1267.
(14) Kwon, Y.; Soon, A.; Han, H.; Lee, H. Shape Effects of Cuprous Oxide Particles on Stability in Water and Photocatalytic Water Splitting. *J. Mater. Chem. A* **2015**, *3*, 156−162.
(15) Kandjani, A. E.; Sabri, Y. M.; Periasamy, S. R.; Zohora, N.; Amin, M. H.; Nafady, A.; Bhargava, S. K. Controlling Core/Shell Formation of Nanocubic P-Cu2O/n-ZnO Toward Enhanced Photocatalytic Performance. *Langmuir* **2015**, *31*, 10922−10930.
(16) Wang, J.-C.; Zhang, L.; Fang, W.-X.; Ren, J.; Li, Y.-Y.; Yao, H.-C.; Wang, J.; Li, Z. Enhanced Photoreduction CO2 Activity over Direct Z-Scheme α-Fe2O3/Cu2O Heterostructures Under Visible Light Irradiation. *ACS Appl. Mater. Interfaces* **2015**, *7*, 8631−8639.
(17) Yuan, G. Z.; Hsia, C. F.; Lin, Z. W.; Chiang, C.; Chiang, Y. W.; Huang, M. H. Highly Facet-Dependent Photocatalytic Properties of Cu2O Crystals Established through the Formation of Au-Decorated Cu2O Heterostructures. *Chem. - Eur. J.* **2016**, *22*, 12548−12556.
(18) Wu, S.-C.; Tan, C.-S.; Huang, M. H. Strong Facet Effects on Interfacial Charge Transfer Revealed through the Examination of Photocatalytic Activities of Various Cu2O-ZnO Heterostructures. *Adv. Funct. Mater.* **2017**, *27*, No. 1604635.
(19) Sasmal, A. K.; Pal, J.; Sahoo, R.; Kartikeya, P.; Dutta, S.; Pal, T. Superb Dye Adsorption and Dye-Sensitized Change in Cu2O-Ag Crystal Faces in the Dark. *J. Phys. Chem. C* **2016**, *120*, 21580−21588.
(20) Zhao, H. Y.; Wang, Y. F.; Zeng, J. H. Hydrothermal Synthesis of Uniform Cuprous Oxide Microcrystals with Controlled Morphology. *Cryst. Growth Des.* **2008**, *8*, 3731−3734.
(21) Sui, Y.; Fu, W.; Yang, H.; Zeng, Y.; Zhang, Y.; Zhao, Q.; Li, Y.; Zhou, X.; Leng, Y.; Li, M.; Zou, G. Low Temperature Synthesis of Cu2O Crystals: Shape Evolution and Growth Mechanism. *Cryst. Growth Des.* **2010**, *10*, 99−108.
(22) Xu, Y.; Wang, H.; Yu, Y.; Tian, L.; Zhao, W.; Zhang, B. Cu2O Nanocrystals: Surfactant-Free Room-Temperature Morphology-Modulated Synthesis and Shape-Dependent Heterogeneous Organic Catalytic Activities. *J. Phys. Chem. C* **2011**, *115*, 15288−15296.
(23) Pang, H.; Gao, F.; Lu, Q. Glycine-Assisted Double-Solvothermal Approach for Various Cuprous Oxide Structures with Good Catalytic Activities. *CrystEngComm* **2010**, *12*, 406−412.
(24) Prabhakaran, G.; Murugan, R. Synthesis of Cu2O Microcrystals with Morphological Evolution from Octahedral to Microrod through a Simple Surfactant-Free Chemical Route. *CrystEngComm* **2012**, *14*, 8338−8341.
(25) Kuo, C.-H.; Huang, M. H. Fabrication of Truncated Rhombic Dodecahedral Cu2O Nanocages and Nanoframes by Particle Aggregation and Acidic Etching. *J. Am. Chem. Soc.* **2008**, *130*, 12815−12820.
(26) Lu, C.; Qi, L.; Yang, J.; Wang, X.; Zhang, D.; Xie, J.; Ma, J. One-Pot Synthesis of Octahedral Cu2O Nanocages via a Catalytic Solution Route. *Adv. Mater.* **2005**, *17*, 2562−2567.
(27) Sun, S.; Zhang, X.; Zhang, J.; Wang, L.; Song, X.; Yang, Z. Surfactant-Free CuO Mesocrystals with Controllable Dimensions: Green Ordered-Aggregation-Driven Synthesis, Formation Mechanism and Their Photochemical Performances. *CrystEngComm* **2013**, *15*, 867−877.
(28) Morgan, P. E. D.; Partin, D. E.; Chamberland, B. L.; Keeffe, M. O. Synthesis of Paramelaconite: Cu4O3. *J. Solid State Chem.* **1996**, *121*, 33−37.
(29) Zhao, L.; Chen, H.; Wang, Y.; Che, H.; Gunawan, P.; Zhong, Z.; Li, H.; Su, F. Facile Solvothermal Synthesis of Phase-Pure Cu4O3 Microspheres and Their Lithium Storage Properties. *Chem. Mater.* **2012**, *24*, 1136−1142.
(30) Su, Y.; Nathan, A.; Ma, H.; Wang, H. Precise Control of Cu2O Nanostructures and LED-Assisted Photocatalysis. *RSC Adv.* **2016**, *6*, 78181−78186.
(31) Su, Y.; Li, H.; Ma, H.; Robertson, J.; Nathan, A. Controlling Surface Termination and Facet Orientation in Cu2O Nanoparticles for High Photocatalytic Activity: A Combined Experimental and Density Functional Theory Study. *ACS Appl. Mater. Interfaces* **2017**, *9*, 8100−8106.
(32) Biesinger, M. C.; Hart, B. R.; Polack, R.; Kobe, B. A.; Smart, R. S. C. Analysis of Mineral Surface Chemistry in Flotation Separation Using Imaging XPS. *Miner. Eng.* **2007**, *20*, 152−162.
(33) Liu, Y.; Ren, F.; Shen, S.; Fu, Y.; Chen, C.; Liu, C.; Xing, Z.; Liu, D.; Xiao, X.; Liu, Y.; Ren, F.; Shen, S.; Fu, Y.; Chen, C.; Liu, C. Efficient enhancement of hydrogen production by Ag/Cu2O/ZnO tandem triple-junction photoelectrochemical cell. *Appl. Phys. Lett.* **2015**, No. 123901.
(34) Mao, Y.; He, J.; Sun, X.; Li, W.; Lu, X.; Gan, J.; Liu, Z.; Gong, L.; Chen, J.; Liu, P.; Tong, Y. Electrochemical Synthesis of Hierarchical Cu2O Stars with Enhanced Photoelectrochemical Properties. *Electrochim. Acta* **2012**, *62*, 1−7.
(35) Debbichi, L.; Marco de Lucas, M. C.; Pierson, J. F.; Krüger, P. Vibrational Properties of CuO and Cu4O3 from First-Principles Calculations, and Raman and Infrared Spectroscopy. *J. Phys. Chem. C* **2012**, *116*, 10232−10237.
(36) de Jongh, P. E.; Vanmaekelbergh, D.; Kelly, J. J. Cu2O: A Catalyst for the Photochemical Decomposition of Water? *Chem. Commun.* **1999**, 1069−1070.

DOI: 10.1021/acsomega.7b01612
ACS Omega 2018, 3, 1939−1945